present field model needs to be confirmed by absolute paleointensity measurements.

3) Even through the use of remanence intensity, paleomagnetic data remain too scarce to allow the elaboration of a reliable global field model. It is necessary to establish first the geographic dependence (on both latitude and longitude) of the amplitude of SV as expressed by σ^2_{SV}.

4) The fundamental assumption in our model is the independence of the magnitude of SV vectors regardless of the longer term variation of the AD even when it decreases to zero. The agreement between our model and the paleomagnetic data presently available suggests that this hypothesis is verified. This conclusion supports the tangential geostrophic model of SV, which, according to theoretical inferences (*27*), implies the independence of the magnitude of SV vectors with respect to the magnitude of the AD. No transfer of the AD energy into other harmonic coefficients seems to occur during reversal, contrary to hypotheses proposed in several reversal models (*7*). We have no evidence for the decrease in the magnitude of SV vectors during reversal that can be inferred from the results of a recent computer simulation of an individual geomagnetic reversal (*28*).

REFERENCES AND NOTES

1. D. Gubbins, *Rev. Geophys.* **32**, 61 (1994); C. G. A. Harrison, *J. Geomagn. Geoelectr.* **47**, 131 (1995).
2. In the literature, no clear physical distinction is made between secular and paleosecular variation processes. According to the model presented in this report, the paleosecular variation is the sum of SV and a slower variation of the AD.
3. R. S. Coe, S. Grommé, E. A. Mankinen, *J. Geophys. Res.* **89**, 1059 (1984); M. Marshall, A. Chauvin, N. Bonhommet, *ibid.* **93**, 11681 (1988); P. Roperch, N. Bonhommet, S. Levi, *Earth Planet. Sci. Lett.* **88**, 209 (1988); S. Levi *et al.*, *ibid.* **96**, 443 (1990).
4. M. Prévot, E. A. Mankinen, R. S. Coe, C. S. Grommé, *J. Geophys. Res.* **90**, 10417 (1985).
5. A. Chauvin, P. Roperch, R. A. Duncan, *ibid.* **95**, 2727 (1990).
6. E. Schnepp, *Geophys. J. Int.* **116**, 688 (1994).
7. K. A. Hoffman, *Science* **196**, 1329 (1977); I. Williams and M. Fuller, *J. Geophys. Res.* **86**, 11657 (1981); D. Gubbins and R. S. Coe, *Nature* **362**, 51 (1993).
8. C. Constable, *J. Geophys. Res.* **95**, 4587 (1990); C. Mary and V. Courtillot, *ibid.* **98**, 22461 (1993).
9. S. Lee, thesis, Australian National University, Canberra (1983).
10. X. Quidelleur, J. P. Valet, V. Courtillot, G. Hulot, *Geophys. Res. Lett.* **21**, 1639 (1994); C. L. Johnson and C. G. Constable, *Philos. Trans. R. Soc. London Ser. A* **354**, 89 (1996).
11. For each flow, we calculated the average direction and remanence intensity after alternating field-cleaning at 10 mT or more. The proportionality between this remanence and the paleofield intensity holds if (i) the primary remanence is a thermoremanent magnetization, which is believed to be the case for basaltic rocks; (ii) secondary magnetizations are absent or were destroyed by the cleaning treatment; and (iii) the effects of mineralogical variations (from one flow to the other) on remanence intensity are averaged out. For the best documented region (Iceland), we demonstrate (in P. Camps and M. Prévot, in preparation) that the viscous secondary remanence left after treatment is negligible. The effects of mineralogical variations are almost entirely averaged out (Figs. 1C and 3C), as attested by the small dispersion of data (all calculated from distinct classes). The database is available through anonymous FTP at ftp.dstu.univ-montp2.fr; use your e-mail address as the password and type cd pub/paleomag.
12. A. Cox, *Geophys. J. R. Astron. Soc.* **8**, 345 (1964). This is the best estimate for κ (which is an inverse measure of the sample dispersion) when the distribution is non-Fisherian.
13. We used the test statistic P_n, as described in *Statistical Analysis of Spherical Data*, N. I. Fisher, T. Lewis, B. J. J. Embleton, Eds. (Cambridge Univ. Press, Cambridge, 1987), p. 165.
14. The formal testing procedures are given in (*13*), p. 122; see also M. A. Stephens, *J. Am. Stat. Assoc.* **69**, 730 (1974). All formal tests (Kolmogorov, Cramer, Kuiper, Watson) strongly reject the Fisher distribution hypothesis (at 99% confidence).
15. A. Cox, *Geophys. J. R. Astron. Soc.* **20**, 253 (1970).
16. M. Prévot and P. Camps, *Nature* **366**, 53 (1993).
17. P. L. McFadden and M. W. McElhinny, *Geophys. J. R. Astron. Soc.* **78**, 809 (1984).
18. R. L. Wilson, P. Dagley, A. G. McCormack, *ibid.* **28**, 213 (1972); L. Kristjansson and I. McDougall, *ibid.* **68**, 273 (1982); J. L. Lin, K. L. Verosub, A. P. Roberts, *Geophys. Res. Lett.* **21**, 525 (1994).
19. R. T. Merrill and M. W. McElhinny, *Rev. Geophys. Space Phys.* **15**, 309 (1977).
20. K. Hirano, in *Encyclopedia of Statistical Sciences*, Kotz *et al.*, Eds. (Wiley, New York, 1982), vol. 7, pp. 647–649.
21. This distribution becomes Fisherian only if $\sigma_{AD} = 0$. See, for example, K. V. Mardia, in *Statistics of Directional Data*, (Academic Press, London, 1972), pp. 232–233. The shape of the observed distribution of directions could be fitted by a Bingham distribution.
22. P. L. McFadden, R. T. Merril, M. W. McElhinny, *J. Geophys. Res.* **93**, 11583 (1988).
23. E. Irving and M. A. Ward, *Pure Appl. Geophys.* **57**, 47 (1964).
24. D. Gubbins, *J. Geophys. Res.* **93**, 3413 (1988).
25. G. Hulot and J. L. Le Mouël, *Phys. Earth Planet. Inter.* **82**, 167 (1994).
26. M. Prévot, M. E. M. Derder, M. McWilliams, J. Thompson, *Earth Planet. Sci. Lett.* **97**, 129 (1990).
27. J. L. Le Mouël, *Nature* **311**, 734 (1984).
28. G. A. Glatzmaier and P. H. Roberts, *ibid.* **377**, 203 (1995).
29. We thank D. K. Bingham, S. C. Bogue, E. Mankinen, P. Roperch, and H. Shibuya for providing unpublished paleomagnetic data and R. Coe for reviewing the first version of this manuscript. This research was completed while P.C. held the position of postdoctoral researcher at the University of California, Santa Cruz, supported by a Ministère de l'Enseignement Supérieur et de la Recherche grant. Contribution CNRS-INSU-DBT "Terre Profonde" 55.

12 March 1996; accepted 13 June 1996

Absorption of Solar Energy in the Atmosphere: Discrepancy Between Model and Observations

Albert Arking

An atmospheric general circulation model, which assimilates data from daily observations of temperature, humidity, wind, and sea-level air pressure, was compared with a set of observations that combines satellite and ground-based measurements of solar flux. The comparison reveals that the model underestimates by 25 to 30 watts per square meter the amount of solar energy absorbed by Earth's atmosphere. Contrary to some recent reports, clouds have little or no overall effect on atmospheric absorption, a consistent feature of both the observations and the model. Of several variables considered, water vapor appears to be the dominant influence on atmospheric absorption.

Recent studies indicate that there are substantial discrepancies between models and observations in the disposition of solar energy within Earth's climate system (*1–6*). Of the global average solar energy incident at the top of the atmosphere (TOA) (342 W m^{-2}), approximately 30% (102 W m^{-2}) is reflected back to space; the remainder (240 W m^{-2}) is absorbed by the atmosphere and the surface. The partitioning of this absorbed energy between the atmosphere and the surface is an important factor in determining the circulation of the atmosphere and the resulting temperature distribution (*7*), and is now the subject of debate.

Comparison of a general circulation model (GCM) with observations at 720 surface sites collected in the Global Energy Balance Archive (GEBA) (*8*) showed that the model overestimates by 10 to 15 W m^{-2} the global average solar flux absorbed by the surface (*1*). This result is consistent with an excess of 9 to 18 W m^{-2} in the downward solar irradiance at the surface in four other models, which were compared with observations at 93 GEBA sites (*2*).

The global mean solar flux absorbed in the atmosphere in four GCMs ranges from 56 to 68 W m^{-2} (*3*). These values are considerably smaller than those derived from observations at ~1000 GEBA sites and extended globally by means of empirical relations, 98 W m^{-2} (*8*), and are closer to the atmospheric absorption value derived from satellite-based estimates of surface flux, 65 to 83 W m^{-2} (*3*). The satellite-based estimates use radiative transfer codes to determine atmospheric absorption, so that comparing GCM absorption with satellite-based absorption is essentially a comparison of models. However, the upper end

Department of Earth and Planetary Sciences, Johns Hopkins University, Baltimore, MD 21218, USA. E-mail: arking@aa.gsfc.nasa.gov

of the range of satellite-based absorption (83 W m^{-2}) has been validated against GEBA surface measurements (9) and is consistent with the analysis presented here.

With models tending to underestimate the amount of solar energy absorbed in the atmosphere, a number of studies have focused on the role of clouds (4–6, *10*, *11*). The effect of a cloud layer on atmospheric absorption varies appreciably with cloud height and optical thickness, solar zenith angle, and underlying surface albedo (*12*). However, in large-scale averages with current radiative transfer models, the overall effect of clouds on atmospheric absorption tends to be small. In essence, the reduced transmission of solar radiation in models of the atmosphere containing clouds is almost entirely attributable to increased reflection to space, with little change in atmospheric absorption. Some recent studies, however, suggest that clouds contribute appreciably to atmospheric absorption (4–6). If the results of those studies—which were based on observations at a few surface sites and from instrumented aircraft—are globally applicable, then clouds contribute to atmospheric absorption an additional 25 W m^{-2} that is not accounted for in the models.

The methods that have been used to show that clouds have a strong effect on atmospheric absorption (4–6) have been questioned (*13*), and strong absorption of solar radiation by clouds is inconsistent with the observed reflectance of clouds (*14*). A reanalysis of one of the data sets used in those studies has shown that clouds have only a small effect on atmospheric absorption (*10*). Analysis of the GEBA data set, combined with an algorithm for computing clear-sky fluxes at the surface, also shows small cloud effects (*11*).

To help resolve this issue, a model is compared with observations based on GEBA surface measurements. This comparison differs from a previous GEBA-based analysis (*11*) in that no attempt is made to determine surface fluxes for clear-sky conditions, which would have introduced a potential source of error.

The observations were extracted from a data set assembled by the World Climate Research Program (WCRP) Surface Radiation Budget Climatology Project (SRB) (*15*). The data set includes the following monthly average measurements from March 1985 to December 1988: (i) downward solar irradiance from 173 surface sites selected from GEBA; (ii) net flux at TOA from the Earth Radiation Budget Experiment (ERBE) (*16*) for all-sky conditions (that is, an average over all measurements) and for clear-sky conditions (an average of measurements where the field of view is determined to be cloud-free); (iii) estimates of surface albedo produced by SRB; (iv) mean cloud cover fraction from the WCRP International Satellite Cloud Climatology Project (ISCCP) (*17*); and (v) total column water vapor, derived from the TIROS Operational Vertical Sounder (TOVS) sensors on the National Oceanic and Atmospheric Administration polar orbiting meteorological satellites (from ISCCP). The use of monthly means, rather than the short–time-scale averages used in the earlier studies (4–6), avoids the problem posed by the variability in surface flux that depends on whether the clouds block the sun when there is partial cloud cover (*13*).

Given the GEBA measurements of downward solar irradiance, the surface albedo is needed to determine the net solar flux at the surface. SRB produces two estimates of surface albedo, one based on the Pinker algorithm (*18*), the other on the Staylor algorithm (*19*); because neither can be considered a superior estimate, both are used here. Although the SRB data set includes satellite-based estimates of the net solar flux at the surface, those variables were not used because they are relatively new and the algorithms for producing them have not been fully validated. Thus, values for the net solar flux at the surface are based on GEBA observations of downward solar irradiance and estimates of surface albedo, the latter having a small overall effect. The fluxes at the surface represent all-sky values; there is no information on what the fluxes would be under clear-sky conditions.

The variables in the observational data set were collocated and averaged by SRB within grid boxes of approximately 280 by 280 km, and I selected only grid points and months for which all of the above data are present. There are a total of 113 spatial grid points contributing data, with some grid boxes containing multiple GEBA surface sites. The grid points are unevenly distributed over the globe; there are only 8 points in the Southern Hemisphere and another 23 points between the equator and 30°N, and most points are within or close to continents. Hence, the observations represent primarily the continents in the north temperate zone. Not all grid points contribute data in each of the 46 months. The full observational data set consists of a total of 2852 data points and is referred to as GEBA-ERBE.

The observations were compared with the model output from version 1 of the

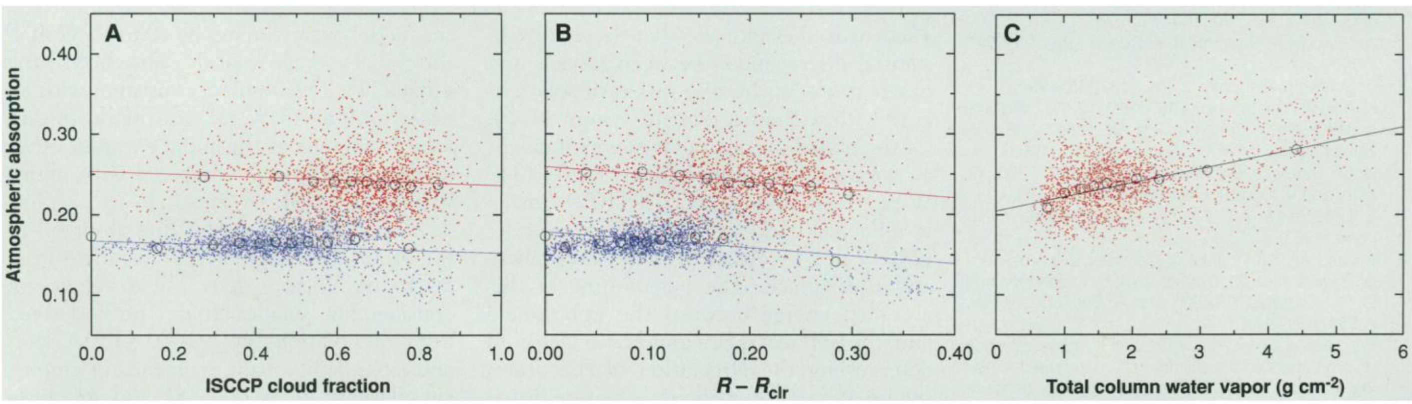

Fig. 1. (**A**) Scatter plot of atmospheric absorption versus ISCCP cloud fraction; (**B**) scatter plot of atmospheric absorption versus ERBE all-sky minus clear-sky albedo at TOA ($R - R_{clr}$). The red data points are from the GEBA-ERBE data set with the average of the surface albedos of Pinker and Staylor; the blue data points are from the GEOS-1 model. Data points are plotted only where the surface albedo satisfies filter F1. The solid lines are derived by linear regression [slopes and their respective explained variances in (A), −0.018 and 0.004 for GEBA-ERBE, −0.015 and 0.019 for GEOS-1; slopes and their respective explained variances in (B), −0.097 and 0.026 for GEBA-ERBE, −0.098 and 0.167 for GEOS-1] (*22*, *23*). Circles are values obtained by binning into 10 bins, with an equal number of data points in each bin. The additional circle on the ordinate axis indicates GEOS-1 clear-sky absorption. (**C**) Scatter plot of atmospheric absorption versus total column water vapor for the GEBA-ERBE data set with the average of the surface albedos of Pinker and Staylor, using filter F1. The solid line is derived by linear regression (slope 0.017, explained variance 0.183), although a square-root dependence would be expected to give a better fit. Circles are values obtained by binning, as described above.

Goddard Earth Observing System (GEOS-1) data assimilation system (*20*). The model was run in a data assimilation mode over a period that included the GEBA-ERBE period. Input to the model consisted of observed pressure heights (essentially, mean layer temperatures), humidity, winds, and sea-level air pressure from satellite, balloon-borne, and ground-based measurements. The model output used here consists of monthly means of surface and TOA fluxes for all-sky and clear-sky conditions, surface albedo, cloud fraction, and total column water vapor, after regridding to match the SRB grid. For each variable of GEBA-ERBE, therefore, there was a matching collocated model variable, plus clear-sky flux at the surface, for which there is no corresponding observation. The data set derived from the model output is referred to as GEOS-1.

The solar flux absorbed by the atmosphere is the difference between the net flux at TOA (Q^T) and the net flux at the surface (Q^S). For GEBA-ERBE, Q^S is related to the downward solar irradiance at the surface ($F^{\downarrow S}$) by $Q^S = (1 - \alpha_s)F^{\downarrow S}$, where α_s is the surface albedo. Comparison of the absorbed solar flux in the model 6 that in the observations shows that the model underestimates the absorbed solar flux in the atmosphere by 25 to 30 W m^{-2} (Table 1). The factor of ~2 difference in SD between the model and the observations may be the result of mismatches between GEBA surface measurements, which are extremely poor spatial samples, and ERBE measurements at TOA (*21*).

To minimize the effects of surface albedo on the results (which were found to be small anyway), three sets of comparisons were made (Table 1): (i) no filter applied to the data (2852 data points); (ii) restriction of data to points where the differences in surface albedo among the Pinker, Staylor, and GEOS-1 values do not exceed 0.1 (filter F1, 1894 data points); and (iii) restriction of data to points where $\alpha_s \leq 0.2$ in each data set (filter F2, 1867 data points). Because the mean incident solar flux (irradiance) at TOA varies with the filter used (from 333 to 352 W m^{-2}) and because there is a small systematic difference between the model and the observations, the entries were normalized to 342 W m^{-2}, the global mean incident solar flux at TOA.

Table 1. Mean and SD of energy absorbed in the atmosphere, normalized to an incident solar flux of 342 W m^{-2} at TOA. GEBA-ERBE-P and GEBA-ERBE-S refer to the GEBA-ERBE data set with the surface albedo estimates of Pinker and Staylor, respectively. Filters F1 and F2 are described in the text.

Filter	Data set	Energy absorbed (W m^{-2})	
		Mean	SD
None	GEBA-ERBE-P	80.1	40.1
	GEBA-ERBE-S	83.8	37.0
	GEOS-1	54.5	19.4
F1	GEBA-ERBE-P	82.4	32.7
	GEBA-ERBE-S	83.1	31.3
	GEOS-1	54.8	16.4
F2	GEBA-ERBE-P	83.6	34.5
	GEBA-ERBE-S	84.1	32.8
	GEOS-1	54.4	16.9

To determine the how much of the 25 to 30 W m^{-2} discrepancy could be attributed to clear-sky absorption and how much to the effect of clouds, atmospheric absorption [defined by $A = (Q^T - Q^S)/I$, where I is the incident solar flux at TOA] is plotted against two independent measures of cloud: cloud fraction from ISCCP (Fig. 1A), and the radiative effect of the cloud at TOA, $R - R_{clr}$ (where R and R_{clr} are the all-sky and clear-sky albedos at TOA, respectively), from ERBE (Fig. 1B). The large discrepancy between the model and observations is practically independent of either cloud measure, and there is little or no correlation between absorption and clouds, either in the model or in the observations. For GEOS-1, where the mean clear-sky atmospheric absorption can be directly computed, there is close agreement between the directly computed mean and the value implied by the regression lines in each plot.

To ensure that the relations shown in Fig. 1, A and B, were not a result of internal correlations with hidden variables that might compensate for what would otherwise be a positive cloud effect, relations involving three other variables that might influence atmospheric absorption were examined: incident solar flux (a proxy for the effect of solar zenith angle), surface albedo, and total column water vapor. Along with either cloud fraction or $R - R_{clr}$, these variables were used as independent variables in a multiple linear regression (*22*), with atmospheric absorption as the dependent variable. Regressions using each of the observed surface albedos were performed with unfiltered data and with F1- and F2-filtered data. The slope representing the relation between atmospheric absorption and cloud fraction was found to be close to zero in each case, never exceeding 0.10. A slope of 0.1 in the relation of atmospheric absorption to $R - R_{clr}$ corresponds precisely to a ratio of 1.1 in the ratio of cloud forcing at the surface to that at TOA, which was found by Cess *et al.* (*4*), Ramanathan *et al.* (*5*), and Pilewskie and Valero (6) to be ~1.5. Thus, the relation between atmospheric absorption and $R - R_{clr}$ derived from the GEBA-ERBE data set is inconsistent with the results of those studies.

In the multiple regressions, the explained variance (*23*) ranged from 21 to 37%, depending on the filter. Comparison of the individual contributions of each independent variable to the total explained variance revealed that total column water vapor is responsible for most of the explained variance. In single regression of atmospheric absorption against total column water vapor, the explained variance ranged from 16 to 33%, with a positive slope (Fig. 1C). In contrast, the model exhibits a weak dependence on total column water vapor, which indicates that the discrepancy between model and observations (25 to 30 W m^{-2} on average) is mostly a function of total column water vapor—the discrepancy increasing with increasing water vapor.

The conclusion is that the GEOS-1 model, which is typical of many GCMs, underestimates the solar flux absorbed in the atmosphere by 25 to 30 W m^{-2}. It is found that clouds do not have a strong effect on atmospheric absorption, and in that respect the model and observations are consistent. The observations indicate there is a strong dependence of atmospheric absorption on total column water vapor, whereas the model does not, which suggests either that the model's parameterization of water vapor absorption is inadequate or that the model fails to account for other atmospheric absorbers at the observation sites that correlate with water vapor (such as absorbing aerosols).

Such a large discrepancy between the model and the observations—if truly global and not merely a characteristic of the observation sites—has important implications for the global energy and hydrological cycle. If more energy is absorbed in the atmosphere than has been suspected, then there is less evaporation from the surface, and correspondingly less precipitation. Also, there would be an effect on both the atmospheric and oceanic circulations, perhaps altering their relative roles in transporting energy from the tropics to higher latitudes.

REFERENCES AND NOTES

1. M. Wild, A. Ohmura, H. Gilgen, *J. Clim.* **8**, 1309 (1995).
2. J. R. Garratt, *ibid.* **7**, 72 (1994).
3. Z. Li, L. Moreau, A. Arking, *Bull. Am. Meteorol. Soc.*, in press.
4. R. D. Cess *et al.*, *Science* **267**, 496 (1995).
5. V. Ramanathan *et al.*, *ibid.*, p. 499.
6. P. Pilewskie and F. P. J. Valero, *ibid.*, p. 1626.
7. J. T. Kiehl, J. J. Hack, M. H. Zhang, R. D. Cess, *J. Clim.* **8**, 2200 (1995).
8. A. Ohmura and H. Gilgen, *Am. Geophys. Union Geophys. Monogr. 75* (1993), p. 93.
9. Z. Li, C. H. Whitlock, T. P. Charlock, *J. Clim.* **8**, 315 (1995).
10. D. G. Imre, E. H. Abramson, P. H. Daum, *J. Appl. Meteorol.*, in press.
11. Z. Li, H. W. Barker, L. Moreau, *Nature* **376**, 486

(1995); Z. Li and L. Moreau, *J. Appl. Meteorol.* **35**, 653 (1996).
12. M.-D. Chou, A. Arking, J. Otterman, W. L. Ridgway, *Geophys. Res. Lett.* **22**, 1885 (1995).
13. A. Arking, M.-D. Chou, W. L. Ridgway, *ibid.* **23**, 829 (1996).
14. G. L. Stephens, *Science* **271**, 1131 (1996).
15. C. H. Whitlock *et al.*, *Bull. Am. Meteorol. Soc.* **76**, 905 (1995).
16. B. Barkstrom *et al.*, *ibid.* **70**, 1254 (1989). Although the ERBE all-sky average for the month is straightforward, the clear-sky average is determined by averaging only those instantaneous measurements within the grid box and within the month for which an algorithm determines that the scenes are cloud-free. Thus, it does not represent what would have been the measurement if clouds were removed, which is what the clear-sky flux represents in a model.
17. W. B. Rossow and R. A. Schiffer, *Bull. Am. Meteorol. Soc.* **72**, 2 (1991).
18. R. Pinker and I. Laszlo, *J. Appl. Meteorol.* **31**, 194 (1992).
19. W. L. Darnell, W. F. Staylor, S. K. Gupta, F. M. Denn, *J. Clim.* **1**, 820 (1988).
20. S. D. Schubert, R. B. Rood, J. Pfaendtner, *Bull. Am. Meteorol. Soc.* **74**, 2331 (1993).
21. SDs for Q^T are ~100 W m^{-2} for both the model and the observations, but for Q^S they are ~75 W m^{-2} for the model and ~100 W m^{-2} for the GEBA observations, which indicates that the additional variability in observed Q^S might be a sampling problem.
22. In calculating means, correlation coefficients, and regression parameters involving ratios—for example, atmospheric absorption and albedo—the data points were appropriately weighted by the incident solar flux at TOA.
23. In multiple linear regression, the dependent variable y is represented by a variable y', which is a linear function of several independent variables x_i. The explained variance is then the ratio of the variance of y' to the variance of y, and it represents the fraction (or percentage) of the original variance contained in y that is contained in or "explained by" y'. Hence, it is a measure of the goodness of the linear fit, and for a perfect fit the explained variance is 100%. In single linear regression there is only one independent variable, and the explained variance (as defined here) is equal to the square of the correlation coefficient.
24. I thank Z. Li, M.-D. Chou, W. Ridgway, R. Cess, T. Charlock, and S. Warren for helpful discussions. Supported by NASA grant NAG 5-2039.

1 April 1996; accepted 18 June 1996

Subnanometer-Diameter Wires Isolated in a Polymer Matrix by Fast Polymerization

Josh H. Golden, Francis J. DiSalvo,* Jean M. J. Fréchet,* John Silcox, Malcolm Thomas, Jim Elman

The preparation and analysis of inorganic-organic polymer nanocomposites consisting of inorganic nanowires and multiwire "cables" in a random-coil organic polymer host is reported. Dissolution of inorganic $(LiMo_3Se_3)_n$ wires in a strongly coordinating monomer, vinylene carbonate, and the use of a rapid polymerization in the presence of a cross-linking agent produce nanocomposites without phase separation. Polymerization of dilute solutions yields a material containing mostly $(Mo_3Se_3^-)_n$ mono- and biwires, 6 to 20 angstroms in diameter and 50 to 100 nanometers long. Polymerization of more concentrated liquid crystalline solutions yields a nanocomposite containing oriented multiwire cables, 20 to 40 angstroms in diameter and up to 1500 nanometers long, that display optical anisotropy and electrical conductivity.

The rational design and fabrication of materials that display "nanowire" or "molecular wire" morphologies is driven by potential applications in nanoscale electronic, optical, and mechanical devices (*1*). Useful properties exhibited by these materials include nonlinear optical phenomena, magnetism, anisotropic conductivity, and dichroism (*2, 3*). Some approaches used in the preparation of inorganic and organic nanofibrillar structures and composites include template synthesis of nanowires within the confines of a porous host matrix, traditional solution synthesis, and the mechanical dispersion of carbon and silica nanotubes within an organic polymer host (*3–7*).

We have prepared a nanocomposite consisting of a rigid rod metallopolymer dispersed in a random coil organic polymer host by using the "monomer as solvent" approach. This technique has been used to prepare nearly monodisperse molybdenum chloride clusters, 10 Å in diameter, isolated from one another in an organic polymer host matrix (*8*). The approach involves the preparation of solutions consisting of inorganic salts dissolved in an organic monomer that are bulk-polymerized in the presence of a cross-linking agent. If the monomer is chemically bound to the metal species and thus serves as a polymerizable ligand, fast solidification and chemical association of the inorganic phase with the supporting organic matrix may be achieved simultaneously. Flory has shown that rigid rods should phase-separate in the presence of a random coil organic polymer, even at low concentrations (*9*). However, the use of a solvating monomer coupled to the fast polymerization of the cross-linking system about the rigid rods kinetically traps the dispersed form. The final concentration of the rigid rods in the solid nanocomposite can be tuned to yield materials that contain individual isotropic nanowires or oriented multiwire "cables." This approach has now been extended to disperse a purely inorganic metallopolymer $(LiMo_3Se_3)_n$ (Fig. 1, A and B) in a random-coil organic polymer poly(vinylene carbonate) [poly(VC)]

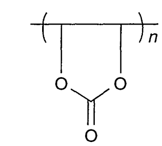

We used $(LiMo_3Se_3)_n$ because it is soluble in polar solvents and has useful linear dichroism and electronic conductivity properties (*10*). The high solvation energy of Li^+ drives the dissolution of $(LiMo_3Se_3)_n$ to produce dark burgundy solutions (absorption maximum at 480 nm) of Li^+ cations and $(Mo_3Se_3^-)_n$ polyanions (*10*). The metallopolymer $(LiMo_3Se_3)_n$ is a member of the $(MMo_3X_3)_n$ (M, an alkali or monovalent main-group metal; X, S or Se or Te) series of metallic linear-chain compounds first described by Potel and co-workers (*11*) and is structurally related to the Chevrel phases (*12*). It is prepared (*10*) as shown below

$$\mathrm{In} + 3\mathrm{Mo} + 3\mathrm{Se} \xrightarrow{1000°\mathrm{C}} \mathrm{InMo_3Se_3}$$

$$\mathrm{InMo_3Se_3} + \mathrm{LiI} \xrightarrow{-\mathrm{InI}} \mathrm{LiMo_3Se_3}$$

The organic component, the polar monomer VC, was chosen because its chemical structure is similar to that of the nonpolymerizable solvent propylene carbonate (*8*), which dissolves $(LiMo_3Se_3)_n$ (*10*). The VC monomer retains the solubilizing property of its nonpolymerizable counterpart and polymerizes to a high molecular weight product in the presence of a free-radical generator (*13*). In addition, poly(VC) is an excellent supporting host for conducting Li salts (*14*).

A dilute inorganic-organic polymer nanocomposite containing mono- and biwires of $(Mo_3Se_3^-)_n$ was prepared by the thermal free-radical polymerization of 10^{-3} to 10^{-4} M VC-$(LiMo_3Se_3)_n$ solutions containing 10% by weight tris(2-hydroxyethyl) isocyanurate triacrylate (the cross-linking agent) and 2 mole percent 2,2′-azobis(2,4-dimethylvaleronitrile) (the free-radical initiator) at 23° to 50°C. The addition of a rapidly curing cross-linking agent to the

J. H. Golden, F. J. DiSalvo, J. M. J. Fréchet, Department of Chemistry, Cornell University, Baker Laboratory, Ithaca, NY 14853, USA.
J. Silcox and M. Thomas, Cornell University Materials Science Center, Clark Hall, Ithaca, NY 14853, USA.
J. Elman, Eastman Kodak Company, Rochester, NY 14650, USA.

*To whom correspondence should be addressed.